NANO LETTERS

Letter

pubs.acs.org/NanoLett

Morphology Control of Nanostructures: Na-Doped PbTe–PbS System

Jiaqing He,*[,†,‡,§] I. D. Blum,[†] Hui-Qiong Wang,[∥] S. N. Girard,[‡] J. Doak,[†] Li-Dong Zhao,[‡] Jin-Cheng Zheng,[∥] G. Casillas,[⊥] C. Wolverton,[†] M. Jose-Yacaman,[⊥] D. N. Seidman,[†,#] M. G. Kanatzidis,*[,‡] and V. P. Dravid*[,†]

[†]Department of Materials Science & Engineering, Northwestern University, Evanston, Illinois 60208, United States

[‡]Department of Chemistry, Northwestern University, Evanston, Illinois 60208, United States

[§]Frontier Institute of Science and Technology, Xi'an Jiaotong University, Xi'an 710054, P. R. China

[∥]Department of Physics, Xiamen University, Xiamen 361005, P. R. China

[⊥]Department of Physics and Astronomy, University of Texas at San Antonio, San Antonio, Texas 78249, United States

[#]Center for Atom-Probe Tomography, Northwestern University, Evanston, Illinois 60208, United States

Supporting Information

ABSTRACT: The morphology of crystalline precipitates in a solid-state matrix is governed by complex but tractable energetic considerations driven largely by volume strain energy minimization and anisotropy of interfacial energies. Spherical precipitate morphologies are favored by isotropic systems, while anisotropic interfacial energies give energetic preference to certain crystallographically oriented interfaces, resulting in a faceted precipitate morphology. In conventional solid–solution precipitation, a precipitate's morphological evolution is mediated by surface anchoring of capping molecules, which dramatically alter the surface energy in an anisotropic manner, thereby providing exquisite morphology control during crystal growth. Herein, we present experimental evidence and theoretical validation for the role of a ternary element (Na) in controlling the morphology of nanoscale PbS crystals nucleating in a PbTe matrix, an important bulk thermoelectric system. The PbS nanostructures formed by phase separation from a PbI_2-doped or undoped PbTe matrix have irregular morphologies. However, replacing the iodine dopant with Na (1–2 mol %) alters dramatically the morphology of the PbS precipitates. Segregation of Na at PbTe/PbS interfaces result in cuboidal and truncated cuboidal morphologies for PbS. Using analytical scanning/transmission electron microscopy and atom-probe tomography, we demonstrate unambiguously that Na partitions to the precipitates and segregates at the matrix/precipitate interfaces, inducing morphological anisotropy of PbS precipitates. First-principles and semiclassical calculations reveal that Na as a solute in PbTe has a higher energy than in PbS and that Na segregation at a (100) PbTe/PbS interface decreases the total energy of matrix/precipitate system, resulting in faceting of PbS precipitates. These results provide an impetus for a new strategy for controlling morphological evolution in matrix/precipitate systems, mediated by solute partitioning of ternary additions.

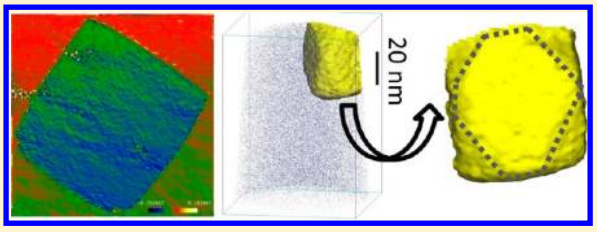

KEYWORDS: *Nanostructures, morphology control, transmission electron microscopy, thermoelectric materials*

A great number of materials properties and phenomena in two-phase systems are governed by the morphological evolution of precipitates in a matrix as a function of temperature, time, composition, and external stimuli, for example, stress.[3−5] Furthermore, the morphology of a precipitate has significant implications for the mechanical, electronic, optical, magnetic, and catalytic properties of materials.[6−8] Considerable efforts have been devoted to the synthesis of nanostructures with a well-controlled morphology in single-phase systems, ranging from nanowires to nanospheres.[9−13] Similarly, there is extensive evidence for morphological control in solid–solution precipitation, where surface anchoring of molecular moieties profoundingly influences the precipitate morphology.

Segregation-induced anisotropic grain-structure is well-known in physical metallurgy.[14−16] Remarkably, however, similar segregation-controlled morphological evolution of precipitates in ternary, quaternary, and so forth systems has not been extensively investigated in nonmetallurgical systems. Theoretical predictions based on the minimization of interfacial free energy and strain energy subject to the constraint of constant volume depend on the size of precipitates because the ratio of elastic strain energy to interfacial free energy is proportional to precipitate size.[3−5,15−17] Such formalisms,

Received: September 16, 2012
Revised: October 13, 2012
Published: October 16, 2012

however, are not applicable in situations where a third element is involved, and its segregation at heterophase interfaces can decrease the interfacial free energy, resulting in segregation-induced morphological control of the precipitates.[14−18]

Herein, we report control of precipitate morphology by the presence of a third element, Na, in a pseudobinary PbTe−PbS system. We find that Na has a much greater solid-solubility in PbS than in PbTe, and it partitions to the PbS precipitates across PbTe/PbS interfaces. Additionally, we find notable segregation of Na at PbTe-matrix/PbS-precipitate interfaces, resulting in highly faceted morphologies, implying anisotropy of heterophase interfacial free energy caused by Na segregation. We also demonstrate that morphological control is governed by the ratio of PbS to Na concentrations and by appropriate thermal processing. By combining scanning/transmission electron microscopy (S/TEM), atom-probe tomography (APT), first-principles calculations, and continuum elasticity modeling, we suggest a rational understanding of the formation of faceted nanostructures in this system. These findings have significant implications for anisotropic morphological evolution in precipitate/matrix systems as in physical metallurgy, such as PbTe/PbS-Na, but also for understanding and controlling the transport properties of nanostructured thermoelectric systems.[19]

We synthesized $Pb_{0.98}Na_{0.02}S_xTe_{1-x}$ (x = 0.04, 0.08, 0.12, 0.16, and 0.30), $Pb_{1-y}Na_yS_{0.12}Te_{0.88}$ (y = 0.005, 0.01, 0.015, and 0.02), and $Pb_{0.98}K_{0.02}S_{0.12}Te_{0.88}$ bulk thermoelectric materials via suitable thermal processing conditions by solid-state reactions at temperatures above the bulk melting points in carbon-coated sealed high-vacuum fused silica tubes. TEM observations reveal a bimodal distribution of PbS precipitate sizes: one set between 2 and 10 nm in nominal diameter (the same below), and the other set is between 20 and 200 nm. The two sets of precipitates are observed in an n-type PbI_2 doped PbTe-PbS system, where all PbS precipitates, regardless of size, are irregularly shaped (Figure 1S in the Supporting Information).[1,2,20] Even when K was introduced as a p-type dopant in the PbTe−PbS system, we observe only irregular morphologies for all precipitates (Figure S1). Significant morphological changes to faceted shapes for midsized PbS precipitates are, however, observed when the K dopant is replaced with Na (~20-200 nm diameter size range).

Figure 1a−e displays low magnification STEM images of 2 mol % Na-doped PbS_xTe_{1-x}(x = 0.30, 0.16, 0.12, 0.08, and 0.04, respectively). A combination of electron diffraction patterns, Figure 1f, energy X-ray disperse spectroscopy (not shown), and APT studies (described below) demonstrate that the different precipitates all have the PbS structure and composition, except for those in Figure 1e, which represent a rock-salt structured phase composed of all three elements Na, Pb, and S, rather than pure PbS or Na_2S. Figure 1a−e reveals changes in precipitate morphology with decreasing PbS concentration. An hexagonal morphology is observed along the PbTe [110] direction for x = 0.30 and 0.16 (Figure 1a and b), while perfect square and rectangular morphologies (>90% of precipitates) are observed with the electron beam parallel to the PbTe [100] axis, for x = 0.12 and 0.08 (Figure 1c and d), and an irregular morphology is observed for x = 0.04 (Figure 1e). The number density of precipitates decreases as the concentration of PbS decreases. We also find that the morphology of the PbS precipitates can be tuned by varying only the Na concentration. For example, for a PbS concentration x = 0.12, TEM reveals that the morphology of the PbS precipitates changes from rectangular

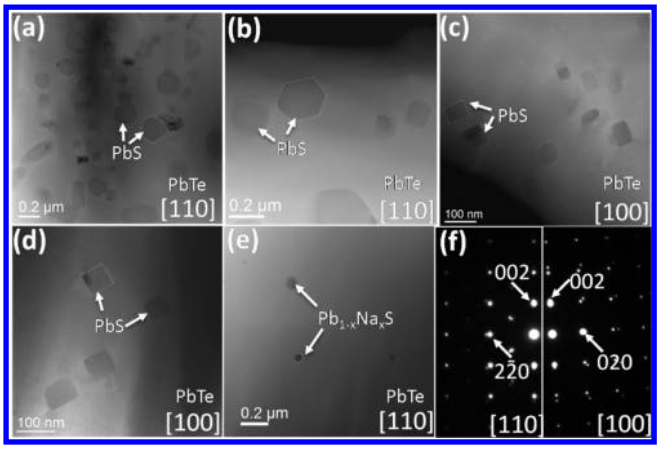

Figure 1. Low magnification TEM images of 2 mol % Na-doped PbTe-PbS X mol % samples (a−e) exhibiting morphological changes of precipitates with different X values: (a) X = 30, (b) X = 16, (c) X = 12, (d) X = 8, (e) X = 4. (f) Electron diffraction patterns with an aperture including matrix and precipitate: left for a and b and right for c and d.

(Na 2 mol %) to a mixture of rectangular and hexagonal for lower concentrations of Na (1−2 mol %) and to irregular shapes at very low Na concentrations (<1 mol %, Figure S2 in the Supporting Information). These observations indicate that the precipitate morphology can be controlled by the ratio PbS/Na. In general, almost all of the precipitates exhibit rectangular and square morphologies when the PbS/Na ratio is between ~4−6: specifically, the 2 mol % Na-doped PbTe−8 mol % PbS and PbTe−12 mol % PbS samples have more than 90% square and rectangular precipitates. When the PbS/Na ratio is greater than 6 or smaller than 4, more truncated square or hexagonal precipitates are observed. Further experiments for 2 mol % Na-doped PbTe−12 mol % PbS samples demonstrate that the precipitate morphology is also controlled by post-aging, such as annealing in furnace, air, or water. As shown in Figure S3 (Supporting Information), precipitates with regular morphologies are observed for furnace cooled samples, and more irregular faceted precipitates are observed for air-cooled samples. When a sample is rapidly cooled by water quenching, only irregularly shaped precipitates are observed.

To understand the formation mechanism of faceted precipitates, further analyses by high-resolution (HR)TEM imaging (Figures 2 and 3) and compositional analyses by APT (Figure 4) were performed. The TEM observations show that the rectangular precipitates form facets parallel to the {100} planes, while the hexagonal precipitates exhibit facets parallel to the {111} (or very few {110}) planes in addition to the {100} planes. Figure 2 shows three typical morphologies of the PbS precipitates, with the electron beam along the [100] direction of PbTe in the 1 mol % Na-doped PbTe−PbS 12 mol % sample. Figure 2a shows a square precipitate projected along the [100] direction with all edges along [001] and [010] directions. The Moiré fringes in the precipitate are due to the matrix/precipitate overlap along the viewing direction. One corner of the precipitate, in Figure 2b, appears cut along the [011] direction, and the same feature is observed for the four corners of the rectangular precipitate displayed in Figure 2c. However, after a careful examination of the precipitate in Figures 2c and APT data (see below), what appears to be a (011) facet is the projection of a (111) facet along the [100] direction. This presence of a (111) facet is confirmed by the

dx.doi.org/10.1021/nl303449x | Nano Lett. 2012, 12, 5979−5984

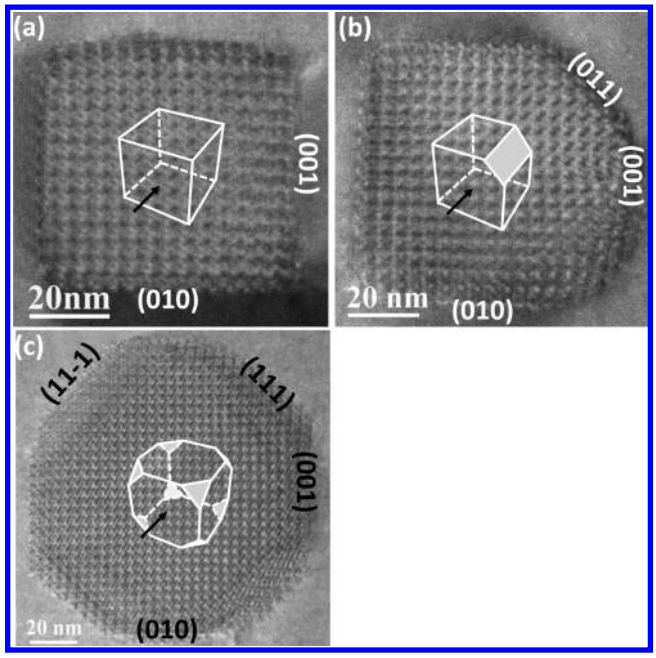

Figure 2. Middle magnification TEM images (a–c) of a 1 mol % Na-doped PbTe–PbS 12 mol % sample displaying three typical projections of PbS precipitates. A schematic of the corresponding precipitate morphology in 3-D space is inserted; the black arrowheads indicate the directions of the TEM observations.

gradually increasing contrast along the [011] direction, while the contrast is sharp along [001] PbTe/PbS interface, indicating an inclined surface. The schematic diagrams of 3-D precipitates exhibiting three different morphologies: a cube, a partially truncated cube, and a fully truncated cube are inserted into the respective images, and each image was obtained along the respective black arrow direction of the 3-D precipitates.

Figure 3a is a HRTEM image of one PbS cube taken close to the edge of a 2 mol % Na-doped PbTe–PbS 8 mol % TEM sample. It displays misfit dislocation contrast at and near the PbTe/PbS interface. Geometric phase analysis (GPA),[21] Figure 3b, confirms the presence of regularly distributed misfit dislocations with the Burger vector 1/2 a[101], with ~4 nm spacing, at or close to the PbTe/PbS interface. The interfacial contrast is unclear due to the large delocalization of the JEOL-2100FEG TEM. To mitigate this imaging artifact, we studied a similar cubic PbS precipitate in another sample using a C_s(probe) corrected JEOL ARM200F microscope in the STEM mode. Figure 3c is a high-angle annular dark-field (HAADF or so-called Z-contrast) image of the cube precipitate in a 2 mol % Na-doped PbTe–PbS 12 mol % sample. The image is of higher quality than the image presented in Figure 3a due to the STEM corrected for spherical aberration. The STEM image exhibits wide dark contrast at the left and top PbTe/PbS interfaces, darker than either the PbTe matrix or the PbS nanostructures. The right and bottom interfaces exhibit clear interfacial contrast and misfit edge dislocations, which are observed in the enlarged image, Figure 3d. This demonstrates that the PbTe/PbS interfacial region is different among the four interfaces. The higher magnification STEM image, Figure 3e, shows that the interfacial region has a transition width of three atomic planes. The lattice parameters of the three layers are shown in Figure 3f, and the lattice parameters of the interfacial region are slightly (1.5%) larger than those of PbS. Energy-dispersive X-ray spectroscopy and electron energy loss

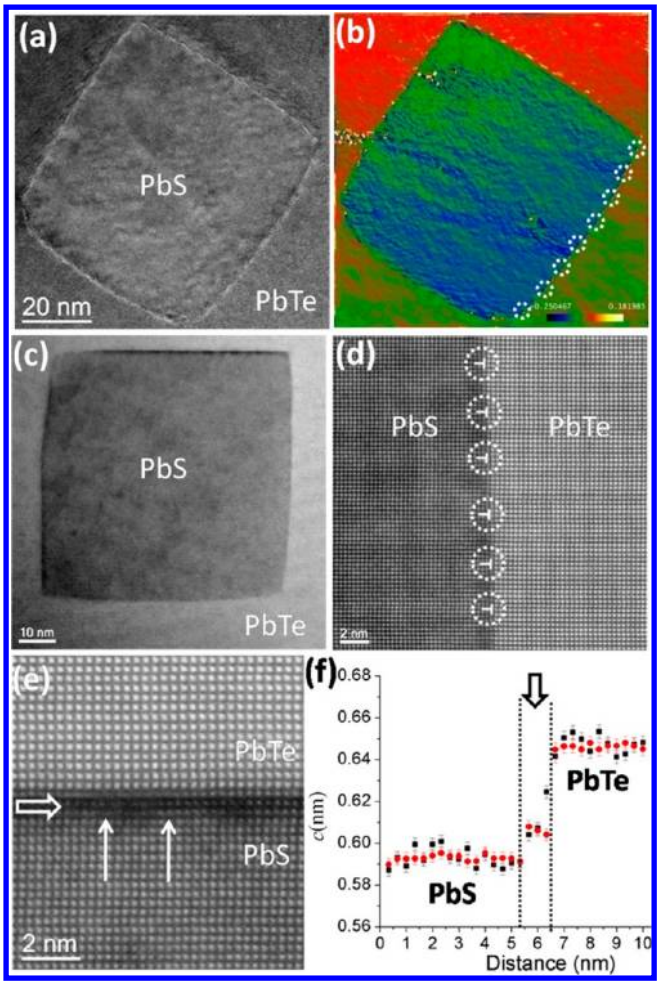

Figure 3. HRTEM image and analysis. (a) HRTEM image of one PbS precipitate in a 2 mol % Na-doped PbTe–PbS 8 mol % sample, (b) GPA analysis of a precipitate exhibiting misfit dislocation cores partially marked by dotted circles, (c) STEM image of the precipitate in a 2 mol % Na-doped PbTe–PbS 12 mol % sample, (d and e) are magnified *Z*-contrast images of the left vertical interface and highest horizontal interface, respectively. Some dislocation cores are indicated by enclosed dotted lines or vertical arrowheads. (f) Evolution of the in-plane (red circles) and out-of-plane (black squares) lattice parameters, with depth along the out-of-plane direction. The Na-rich layer is indicated by the white arrow.

spectroscopy analyses in the TEM did not detect significant differences between the interfacial and precipitate compositions due to their limited sensitivities; therefore we utilized APT for quantitative composition analyses of the interfacial region.

Analyses of the 1 mol % Na-doped PbTe–PbS 12 mol % sample by APT indicates the presence of a S-rich precipitate, Figure 4a. For the sake of clarity, only 3% of the detected Pb atoms are displayed in the 3-D reconstruction. The morphology of the PbS precipitate is highlighted using a 20 at. % S isoconcentration surface. The precipitate is only partially contained within the analyzed volume. Figure 4a shows the isoconcentration surface of the same precipitate, as observed from a [100] direction. These two images of the precipitate demonstrate that its morphology is consistent with a truncated cube. The large facets are parallel to the {100} planes, while the smaller facets are parallel to the {111} planes, confirming the general observations made by TEM for this composition. The compositions of the matrix and precipitate are listed in Table

dx.doi.org/10.1021/nl303449x | *Nano Lett.* 2012, 12, 5979–5984

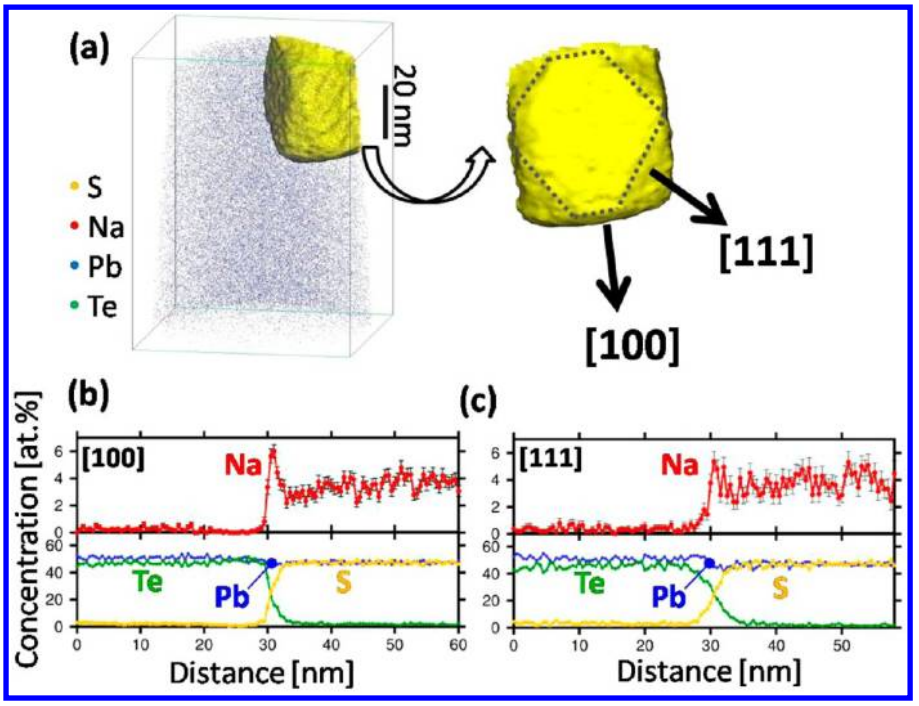

Figure 4. Composition analyzed by atom-probe tomography (APT). (a) Three-dimensional (3-D) reconstruction of a volume. Only 3% of the detected Pb atoms are displayed (blue dots) for clarity. The yellow isoconcentration surface corresponds to 20 at. % S and highlights the precipitates' interfaces. (b) Atomic concentration profiles of Na (red), S (yellow), Pb (blue), and Te (green) across the (100) and (111) interfaces.

S1 (Supporting Information).The measured compositions are consistent with the compositions PbTe and PbS for the matrix and the precipitate, respectively. The Na concentration is 3.49 at. % in the precipitate, while it is only 0.33 at. % in the matrix, yielding a partitioning coefficient of $Na^{PbS}/Na^{PbTe} = 10.6$.

Concentration profiles were measured perpendicular to two interfaces: parallel to the (100) plane (Figure 4b), and to the (111) plane (Figure 4c). No peak corresponding to Te ions are observed in the mass spectrum of the PbS precipitate (not shown). Thus, the Te concentration measured in the precipitate corresponds mainly to background noise. In the case of the (100) interface, Na segregates to a maximum concentration of 5 at. %. The uncertainties of the concentration are, however, higher in the case of the (111) interface because of the smaller area used for calculating the concentration profile.

Na segregation at the precipitates' interfaces is quantified by the relative Gibbsian interfacial excess, which corresponds to the excess number of solute atoms per unit area of interface compared to the number of atoms that would be present in the absence of segregation. Atom-probe tomography (APT) is the only direct method to measure this quantity.[22] We employed Cahn's elegant formalism[23,24] to calculate the interfacial area, which involves placing two surfaces on both sides of the interface, between which the number of atoms of each species is counted. In Cahn's formalism the Gibbsian interfacial excess of Na with respect to Te and S is given by:

$$\Gamma_{Na}^{Te,S} = N_{Na} - [N_{Te}(X_{Na}^{PbTe}X_{S}^{PbS} - X_{Na}^{PbS}X_{S}^{PbTe}) - N_{S}(X_{Na}^{PbTe}X_{Te}^{PbS} - X_{Na}^{PbS}X_{Te}^{PbTe})] / (X_{Te}^{PbTe}X_{S}^{PbS} - X_{Te}^{PbS}X_{S}^{PbTe}) \quad (1)$$

where X_i^j is the atomic fraction of i in phase j, measured in the vicinity of the interface and N_i is the number of atoms i counted between the two surfaces. The result is then corrected for the detection efficiency of the APT, which is 50%. Values of 3.79 ± 0.30 and 3.03 ± 0.47 atom nm^{-2} were found for the (100) and (111) interfaces, respectively, indicating significant segregation of Na at both interfaces. For comparison, the atomic densities of the (100) and (111) PbTe planes are 9.64 and 5.57 at nm^{-2}, respectively, which, if projected on a unique atomic plane, the two interfacial excesses correspond to a coverage of 39 ± 3 and 54 ± 8% of the (100) and (111) planes of PbTe, respectively.

To further understand the physical and chemical effects of adding Na to the interfaces between PbS and PbTe, we performed first-principles density functional theory (DFT) calculations of these binary and ternary interfaces.[25−27] In particular, we are interested in determining whether equilibrium thermodynamics can account for: (i) the Na partitioning to PbS; (ii) Na segregation at the PbTe/PbS interfaces; and (iii) the {100} faceting observed for Na-doped PbS precipitates. Details of the DFT calculations are in the Supporting Information. We modeled the (100) interface between PbTe/PbS with a periodic cell containing six layers of PbS and six layers of PbTe, forming two coherent interfaces. We calculated possible Na defect structures in both PbS and PbTe and found Na_{Pb} to be the lowest energy defect in both PbS and PbTe. Consequently, we used Na_{Pb} as the defect structure for all calculations of Na in PbS, PbTe, as well as for the PbTe/PbS interface. Partitioning energies were calculated by substituting one Pb atom for Na in both PbS and PbTe. Segregation energies, as well as changes in the (100) interfacial energies were calculated as a function of distance from the PbTe/PbS interface by substituting various Pb atoms in the interfacial cell with Na atoms.

From the above calculations we find that (i) Na partitions to PbS over PbTe, in agreement with experimental APT results. We further find that (ii) Na prefers to segregate at the PbTe side of the PbTe/PbS (100) coherent interface (Table S4 in

dx.doi.org/10.1021/nl303449x | Nano Lett. 2012, 12, 5979−5984

Supporting Information). Finally, we find that (iii) the (100) coherent interfacial energy between PbS and PbTe is decreased by the addition of Na at the PbS side of the interface and increased by the addition of Na at the PbTe side of the interface. Thus, the dramatic changes in PbS precipitate morphology that occur upon the addition of Na to PbS-PbTe can be explained by the energetics of PbTe/Na PbS-interfaces.

To further investigate the change in PbS precipitate morphology with Na concentration, we used a semiquantitative elasticity model to compare the elastic energies of cuboidal and spherical precipitates in the matrix.[28−30] Details of the elasticity analysis are in the Supporting Information. We represent the geometry of a precipitate as a supersphere,[28] a 3-D object that varies between a sphere and a cube as a function of an order parameter. Using Eshelby's method,[30] the inclusion problem for this superspherical geometry has been solved for the case of shear stress-free transformation strains.[28] Under these conditions for shear strains (similar to Figure 3f), the ratio of the elastic energy of a cuboidal precipitate to the elastic energy of a spherical precipitate reduces to a function of the material's Poisson ratio, assuming it is the same in the matrix and in the precipitate.[28] Using an estimate of the Poisson ratio for PbS doped with 5 mol % Na, we find the ratio of cuboidal-to-spherical elastic energies to be 0.93, indicating that, according to strain energy considerations, the cuboidal shape is favored compared to the spherical shape. Since the elastic energy of a precipitate is proportional to its volume and the interfacial energy of a precipitate scales with its surface area, the elastic contribution dominates at large precipitate sizes.

In summary, we report successful control of the morphology of PbS precipitates within a PbTe matrix by adding Na as a solute. The detailed investigations demonstrate that Na segregation at specific PbTe-matrix/PbS-precipitate interfaces is responsible for the faceting of PbS precipitates. This is likely an entirely new strategy and is possibly a new way to control nanostructure morphology in (pseudo) binary systems, that is, by the partitioning of a ternary addition to a nominally binary system. Conceptually, the Na in this system appears to play the role of the surfactant capping ligand in conventional nanocrystal formation from organic solutions such as in CdSe and PbSe, among others. By controlling the nature of the capping ligand and by combining more than one capping ligand it has been possible to control the size and the morphology of these materials with highly exotic morphologies including nanostars, nanodisks, nanowires, tetrapods, and branched wires to name a few. In the more challenging solid-state systems, such as PbTe−PbS, the use of Na and other dopants separately and in combination may open new pathways for similar size and morphology control.

■ ASSOCIATED CONTENT

Supporting Information

Experimental details, characterization, and calculations. This material is available free of charge via the Internet at http://pubs.acs.org.

■ AUTHOR INFORMATION

Corresponding Author

*E-mail: jiaqing-he@northwestern.edu, m-kanatzidis@northwestern.edu, and v-dravid@northwestern.edu.

Notes

The authors declare no competing financial interest.

■ ACKNOWLEDGMENTS

This research is based upon work supported as part of the Revolutionary Materials for Solid State Energy Conversion, an Energy Frontier Research Center funded by the U.S. Department of Energy, Office of Science, Office of Basic Energy Sciences under Award Number DE-SC0001054. Transmission electron microscopy work was performed in the (EPIC) (NIFTI) (Keck-II) facility of NUANCE Center at Northwestern University. The NUANCE Center is supported by NSF-NSEC, NSF-MRSEC, Keck Foundation, the State of Illinois, and Northwestern University. The atom-probe tomography and instrumentation at the Northwestern University Center for Atom-Probe Tomography (NUCAPT) were acquired with funding from NSF-MRI (DMR-0420532), ONR-DURIP (N00014-0400798, N00014-0610539, N00014-0910781), the MRSEC program (DMR-1121262), and ISEN at Northwestern University. Work at Xiamen University was supported by SRFDP (Grant No.20090121120028 and 20100121120026) and the National Science Foundation of China (Grant No. U1232110). This work was also supported by the National Science Foundation (NSF) PREM (DMR-0934218).

■ REFERENCES

(1) He, J.; Girard, S. N.; Kanatzidis, M. G.; Dravid, V. P. *Adv. Funct. Mater.* **2010**, *20*, 764−772.
(2) Girard, S. N.; He, J.; Li, C.; Moses, S.; Wang, G.; Uher, C.; Dravid, V. P.; Kanatzidis, M. G. *Nano Lett.* **2010**, *10*, 2825−2831.
(3) Baldan, A. *J. Mater. Sci.* **2002**, *37*, 2379−2405.
(4) Dahmen, U.; Xiao, S. Q.; Paciornik, S.; Johnson, E.; Johansen, A. *Phys. Rev. Lett.* **1997**, *78*, 471−474.
(5) Hamilton, J. C.; Leonard, F.; Johnson, E.; Dahmen, U. *Phys. Rev. Lett.* **2007**, *98*, 236102.
(6) Yang, P. D. *Nature* **2012**, *482*, 41−42.
(7) Huang, W. C.; Lyu, L. M.; Yang, Y. C.; Huang, M. H. *J. Am. Chem. Soc.* **2012**, *134*, 1261−1267.
(8) LaGrow, A. P.; Ingham, B.; Cheong, S.; Williams, G. V. M; Dotzler, C.; Toney, M. F.; Jefferson, D. A.; Corbos, E. C.; Bishop, P. T.; Cookson, J.; Tilley, R. D. *J. Am. Chem. Soc.* **2012**, No. 134, 855−858.
(9) Morales, A. M.; Lieber, C. M. *Science* **1998**, *279*, 208−211.
(10) Pan, Z. W.; Dai, Z. R.; Wang, Z. L. *Science* **2001**, *291*, 1947−1949.
(11) Ebbesen, T. W.; Ajayan, P. M. *Nature* **1992**, *358*, 220−222.
(12) Sun, Y. G.; Xia, Y. N. *Science* **2002**, *298*, 2176−2179.
(13) Saito, Y.; Matsumoto, T. *Nature* **1998**, *392*, 237−237.
(14) Thompson, M. E.; Su, C. S.; Voorhees, P. W. *Acta Metall. Mater.* **1994**, *42*, 2107−2122.
(15) Johnson, W. C.; Berkenpas, M. B.; Laughlin, D. E. *Acta Metall.* **1988**, *36*, 3149−3162.
(16) Onaka, S.; Kobayashi, N.; Fujii, T.; Kato, M. *Mater. Sci. Eng. A* **2003**, *347*, 42−49.
(17) Ribis, J.; de Carlan, Y. *Acta Mater.* **2012**, *60*, 238−252.
(18) Johnson, W. C.; Cahn, J. W. *Acta Metall. Mater.* **1984**, *32*, 1925−1933.
(19) Girard, S. N.; He, J. Q.; Zhou, X.; Shoemaker, D.; Jaworski, C.; Uher, C.; Dravid, V. P.; Heremans, J. P.; Kanatzidis, M. G. *J. Am. Chem. Soc.* **2011**, *133*, 16588−16597.
(20) Androulakis, J.; Lin, C.-H.; Kong, H.-J.; Uher, C.; Wu, C.-I.; Hogan, T.; Cook, B. A.; Caillat, T.; Paraskevopoulos, K. M.; Kanatzidis, M. G. *J. Am. Chem. Soc.* **2007**, *129*, 9780−9788.
(21) Hytch, M. J.; Snoeck, E.; Kilaas, R. *Ultramicroscopy* **1998**, *74*, 131−146.
(22) Dregia, S. A.; Wynblatt, P. *Acta Metall. Mater.* **1991**, *39*, 771−778.

(23) Sutton, A. P.; Balluffi, R. W. *Interfaces in Crystalline Materials*; Clarendon Press: Oxford, U.K., 1996; p 349.
(24) Cahn, J. W. *Interfacial Segregation*; Johnson, W. C., Blakely, J. M., Eds.; American Society of Metals: Meterals Park, 1979; p 3.
(25) Hohenberg, P.; Kohn, W. *Phys. Rev.* **1964**, *136*, B864−B871.
(26) Kohn, W.; Sham, L. J. *Phys. Rev.* **1965**, *140*, A1133−A1138.
(27) Kresse, G.; Furthmuller, J. *Phys. Rev. B* **1996**, *54*, 11169−11186.
(28) Onaka, S. *Philos. Mag. Lett.* **2001**, *81*, 265−272.
(29) Lee, J. K.; Johnson, W. C. *Phys. Status Solidi A* **1978**, *46*, 267−272.
(30) Eshelby, J. D. *Proc. R. Soc. London, Ser. A* **1957**, *241*, 376−396.